Analyses of $\pi^{\pm}$-nucleus elastic scattering data at $T_\pi = 40$, 30, 20 MeV using a suggested scaling method

Z.F. Shehadeh* and R.M. El-Shawaf
Physics Department, Taif University, Taif, Zip Code 21974, Saudi Arabia
**e-Mail: zfs07@hotmail.com*

Received 11 December 2017; accepted 1 February 2018

The data for elastically scattered charged pions from few nuclei, namely ^{12}C, ^{16}O, ^{28}Si, ^{32}S, ^{40}Ca, ^{56}Fe, ^{58}Ni, and ^{90}Zr have been analyzed by obtained potentials using a suggested scaling procedure. Originally the $\pi^{\pm}$ - ^{12}C elastic scattering data at 50 MeV was nicely fitted by a parameterized simple local optical potential extracted from available phase shifts using inverse scattering theory. The potential parameters of the $\pi^{\pm}$ - ^{12}C systems were scaled to $\pi^{\pm}$ - ^{16}O systems and then successively to other few systems covering the scattering of charged pions from target nuclei, namely $\pi^{\pm}$ - ^{28}Si, $\pi^{\pm}$ - ^{32}S, $\pi^{\pm}$ - ^{40}Ca, $\pi^{\pm}$ - ^{56}Fe, $\pi^{\pm}$ - ^{58}Ni and $\pi^{\pm}$ - ^{90}Zr. The obtained scaled potentials showed a remarkable success in explaining the available measured elastic differential cross sections, and in predicting other ones for the systems under consideration. The reaction cross sections have been calculated for all these systems at the three incident pion's kinetic energies, $T_\pi = 40$, 30, 20 MeV. Unfortunately, experimental reaction cross sections are totally absent or cloudy and unconfident. As such, and at this stage, we consider our calculated values useful and pending for future investigations. For the systems and energies considered herein, simple scaling relations are well established. This will be beneficial in analyzing similar nuclear scattering data, as low-energy pion-nucleus and kaon-nucleus elastic scattering data; and, hopefully, in explaining pionic atom data.

Keywords: Pion-nucleus potential; Klein-Gordon equation; elastic scattering; inverse scattering theory; phase shift analysis; scaling method; low-energy physics.

PACS: 25.80.Dj; 11.80.-m; 24.10.Ht

1. Introduction

Due to the mechanism of pion-nucleon interaction, with the pion's mean free path associated with the pion's incident kinetic energy T_π, the pion-nucleus elastic-scattering has been classified into three major energy bins [1], namely (I) the high energy region, $T_\pi > 400$ MeV, (II) the delta resonance energy region, $100 < T_\pi \leq 400$ MeV, and (III) the low energy region, $T_\pi \leq 100$ MeV.

In region I, the pion is the best and most sensitive probe of spatial distributions in a nucleus. The pion is spinless; and it penetrates deeply inside the nucleus because pion-nucleon two-body interaction is weak. In fact, it is one of the most penetrating of the strongly interacting particles. Also it is a preferred probe, compared to the proton, as no need to make antisymmetrization with the nucleons inside a nucleus. In addition, it is the best spectroscopic tool to investigate the many overlapping resonances that do exist. Nevertheless, the presence of unconventional phenomena as mesonic current contributions and modified nucleon properties in the medium could be tested [2].

In region II, the pion's mean free path is small and it is comparable to the inter-nucleon distance [3]. So the pion is completely absorbed at the surface of the target nucleus, *i.e.* the scattering involves the nuclear surface. As such, the pion is an adequate probe for gleaning important nuclear peripheral information.

To facilitate the study of region III, it has been subdivided into two energy sub-regions: (III-a) the transition energy region, $50 < T_\pi \leq 100$ MeV, and (III-b) the very low energy region, $T_\pi \leq 50$ MeV. Here we are investigating the elastic scattering of the nuclear systems $\pi^{\pm}$ - ^{12}C, ^{16}O, ^{40}Ca at $T_\pi = 20$, 30, 40 MeV, $\pi^{\pm}$ - ^{90}Zr at $T_\pi = 20$, 30 MeV, $\pi^{\pm}$ - ^{58}Ni and $\pi^{\pm}$ - ^{90}Zr at $T_\pi = 40$ MeV, *i.e.* in the very low energy region. In this sub- energy region, the pion mean free path is much greater than the inter-nucleon distance which allows the pion to penetrate deeply inside the nucleus [4]. As such the pion is considered the most suitable and best informative probe for studying nuclear structure and revealing nuclear structure effects. It is worthy to point out that nuclear structure effects are obscured in the resonance region.

Recently we have analyzed low-energy pion-nucleus elastic scattering data using a suggested scaling method, based on the results of the inverse scattering theory using available phase shifts for both $\pi^{\pm}$ - ^{12}C and $\pi^{\pm}$ - ^{16}O nuclear systems [5]. It was obvious that the three changed potential parameters, R_0, V_1 and W_3, depend on the atomic mass of the target nucleus. As such, the scaling procedure for the three potential parameters, from a certain pion-nucleus system to a nearby one, became visible. Using the scaled potential parameters for $\pi^{\pm}$ - ^{16}O system from the potential parameters of $\pi^{\pm}$ - ^{12}C system at several bombarding energies below 100 MeV, namely at $T_\pi = 13.9$, 20.0, 30.0, 35.0, 40.0, 50.0, 60.0, 65.0, 80.0 MeV in our adopted potential, our results have shown a nice agreement between the calculated differential and reaction cross sections and the measured values. Moreover, the real and imaginary parts of the scaled potential agree with the inverted potential points obtained from available phase shifts using the inverse scattering theory [6]. The obtained good results were a strong stimulus to investi-

gate the scattering of both charged pions from different target nuclei and isotopes, namely ^{16}O, ^{28}Si, ^{30}Si, ^{32}S, ^{34}S, ^{40}Ca, ^{48}Ca, ^{56}Fe, ^{58}Ni, ^{64}Ni, and ^{90}Zr, at one bombarding energy, $T_\pi = 50.0$ MeV [7]. The obtained good results of this investigation have supported the use of the scaling method, which is our new proposed method, in determining low-energy pion-nucleus reliable potentials. These determined potentials proved the strength, capability and reliability of the scaling method as they provided nice fits to the differential and integral cross sections; and showed a very reasonable agreement with the inverted potential points. As far, the uniqueness of the scaling method appears clearly in obtaining the correct potentials for low-energy pion-nucleus systems with no available shifts. At this stage, and for integrity and completeness, the achieved successful results formed a strong inducement to extend using our suggested scaling method to analyze several pion-nucleus elastic scattering data at few low energies, namely $T_\pi = 20.0$, 30.0, 40.0 MeV. Once more, this allows for an important additional test for the correctness, strength and reliability of this new method in obtaining the scaled potential parameters and, then, the correct potentials for other pion-nucleus scattering cases. Here in this investigation, we will use the scaling method to obtain the optical potentials, with real and imaginary parts, required to explain the $\pi^{\pm} - {}^{12}$C, ^{16}O, ^{40}Ca, ^{56}Fe, ^{58}Ni, and ^{90}Zr available data at the three energies 20, 30 and 40 MeV. Having in mind to submit our scaling method as a patent, we strongly believe that this study forms a valuable test and a complementary witness for the success of our scaling method.

In Sec. 2, theory is briefly overviewed. In Sec. 3, results and discussion are presented. In the last section, Sec. 4, the conclusions are summarized.

2. Theory

This work is a continuation to our recent work [5,7], and, as such, the theoretical background and theoretical relations are as already outlined and discussed before. Accordingly, a brief overview is provided here for completeness.

The potential adopted here, $V(r)$, is the well-known one which is composed of the nuclear part, $V_N(r)$, and the Coulomb part, $V_C(r)$:

$$V(r) = V_N(r) + V_C(r). \tag{1}$$

The analytical form of the nuclear part is given by :

$$V_N(r) = \frac{V_0}{1+\exp\left(\frac{r-R_0}{a_0}\right)} + \frac{V_1}{\left[1+\exp\left(\frac{r-R_1}{a_1}\right)\right]^2} + i\frac{W_3\exp\left(\frac{r-R_3}{a_3}\right)}{\left[1+\exp\left(\frac{r-R_3}{a_3}\right)\right]^2} \tag{2}$$

where the three terms are the attractive Woods-Saxon (WS), the repulsive Squared Woods-Saxon (SWS), and the surface Woods-Saxon, respectively. The Coulomb term, $V_C(r)$, is given by:

$$V_C(r) = \begin{cases} \frac{\pm Z_T e^2}{8\pi\varepsilon_0 R_C}\left(3-\frac{r^2}{R_C^2}\right) & r \le R_C \\ \frac{\pm Z_T e^2}{4\pi\varepsilon_0 r} & r > R_C \end{cases} \tag{3}$$

which represents the interaction between a point charge, *i.e.* the incident charged pion, and a uniformly insulating charged sphere, *i.e.* the target nucleus of atomic number Z_T. The appearing symbols e^2, ε_0 and R_C in Eq. (3) are the squared electron charge, permittivity of free space, and the Coulomb radius. In nuclear units $e^2/4\pi\varepsilon_0 = 1.44$ MeV. As usual, R_C is numerically obtained from $R_C = 1.2A^{1/3}$ with A is the target atomic mass in atomic mass units.

To achieve our goals in obtaining differential and reaction cross sections, $d\sigma/d\Omega$ and σ_r, respectively, without facing mathematical singularities or computational difficulties, $V(r)$ is inserted into the transformed radial part of Klein-Gordon equation:

$$\left[\frac{d^2}{dr^2} + \frac{2(\ell+1)}{r}\frac{d}{dr} + k^2 - U(r)\right]\varphi_{nl}(r) = 0 \tag{4}$$

with k^2 and $U(r)$ are given by

$$k^2 = (E^2 - m^2c^4)/\hbar^2c^2 \tag{5}$$

$$U(r) = \frac{2E}{\hbar^2c^2}[V(r)V^2(r)/2E] \tag{6}$$

All potential quantities, constants and scaled potential parameters, appearing explicitly or implicitly in the above equations are substituted by their numerical values. For emphasis, the quantities E, m, $\hbar$ and c are the actual pion total energy, effective pion mass, reduced Planck constant and the velocity of electromagnetic wave in vacuum, respectively.

It is well-know that the phase shift, δ_ℓ, for each contributing partial waves ℓ, is an important ingredient in the definitions of the elastic differential cross section, $d\sigma/d\Omega$:

$$d\sigma/d\Omega = |f(\theta)|^2 \tag{7}$$

where $f(\theta)$ is the full elastic scattering amplitude at angle θ in the center of mass system. Mathematically, it is expressed as:

$$f(\theta) = f_c(\theta) + \frac{1}{2ik}\sum_{\ell=0}^{\infty}(2\ell+1)e^{2i\sigma_\gamma} \times [e^{2i\delta_\ell} - 1]P_\ell(\cos\theta) \tag{8}$$

where $f_c(\theta)$ is the pure Coulomb scattering amplitude, $P_\ell(\cos\theta)$ are Legendre polynomials, and σ_γ is the Coulomb phase shift defined by [8]:

$$\sigma_\gamma = \text{arg}\Gamma\left(\gamma + \frac{1}{2} + i\eta\right) - \frac{1}{2}\pi\left(\gamma - \frac{1}{2} - \ell\right) \tag{9}$$

with the dimensionless parameter γ:

$$\gamma = \sqrt{\left(\ell + \frac{1}{2}\right)^2 - Z_T^2\alpha^2} \tag{10}$$

Also δ_ℓ appears solely in the definition of the reaction cross section, σ_r:

$$\sigma_r = \frac{\pi}{k^2}\sum_{\ell=0}^{\infty}(2\ell+1)[1-|S_\ell|^2] \tag{11}$$

where $S_\ell = e^{2i\delta_\ell}$ is the S-matrix, and δ_ℓ is complex.

The determination of δ_ℓ is usually done by matching the inner and outer solutions of Eq. (4) at the matching radius $r = R$, *i.e.* at the surface of the nucleus. The inner solution is obtained by integrating the equation numerically from the origin $r = 0$ to $r = R$ using Numerov's method [9]. On the otherhand, the outer solution, *i.e.* for $r \geq R$, considered here is the usual and familiar Coulomb wave function:

$$\varphi_{n\ell} = \frac{1}{(kr)^{\ell+1}}\left\{F_\ell(\eta,kr) + \frac{\exp(2i\delta_\ell)-1}{2i} \times [G_\ell(\eta,kr) + iF_\ell(\eta,kr)]\right\} \tag{12}$$

where F_ℓ and G_ℓ are the relativistic regular and irregular Coulomb wave functions [10], respectively; and the parameter η is Sommerfeld parameter defined as:

$$\eta = \frac{Z_T\alpha E}{k} \tag{13}$$

where α is the fine structure constant.

3. Results and Discussion

As pointed out in our previous work [2,5,7], the scaling method has been successful in obtaining the correct potential parameters capable of providing nice agreements between theory and experiment for alpha-nucleus [11] and nucleus-nucleus [12,13] nuclear systems. In addition, the scaling method is supported by Energy-Density Functional (EDF) theory [13]. Recently it has been also successful in determining the correct potential parameters for pion-nucleus systems in the low energy region. The extent of success, strength, capability and reliability of the scaling method are examined, here, by explaining the elastic-scattering angular distributions data for the pion-nucleus systems under consideration, namely $\pi^\pm$ - ^{12}C, ^{16}O, ^{40}Ca at $T_\pi = 20$, 30, 40 MeV $\pi^\pm$ - ^{90}Zr at $T_\pi = 20$, 30 MeV, π^- - ^{58}Ni and π^- - ^{90}Zr at $T_\pi = 40$ MeV. It is of importance to notice that these systems include a) bombarding pions with different polarities, b) different incident pion's kinetic energies, and c) different target nuclei spanning the periodic table. Nice fits, using scaled pa-

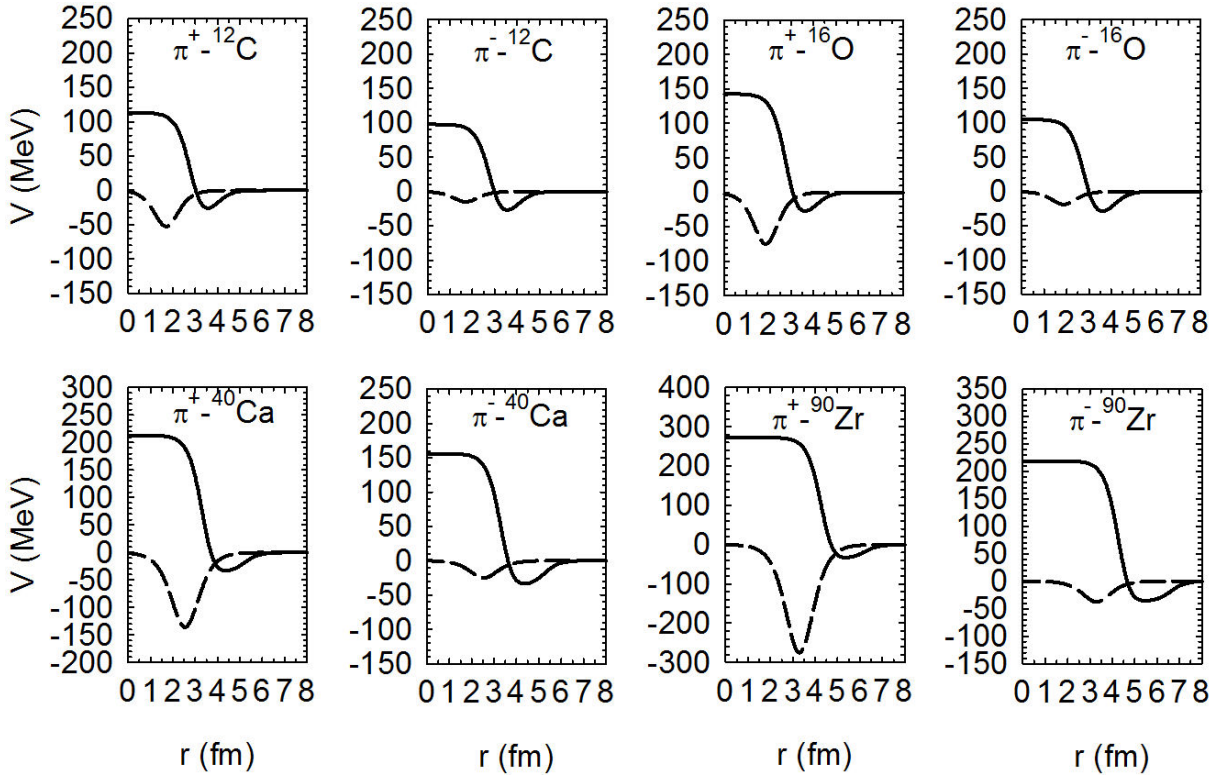

FIGURE 1. The real and imaginary parts of the scaled potentials, drawn as solid and dashed lines, respectively, used in analyzing $\pi^\pm$ - ^{12}C, ^{16}O, ^{40}Ca and ^{90}Zr elastic scattering data at 20 MeV. Unfortunately, there are no available phase shifts.

TABLE I. The optical potential parameters R_0 (in fm), V_1 (in MeV), W_3(in MeV), R_1(in fm), R_3(in fm) and a_3(in fm) used in Eq. (2) for 20 MeV incident charged pions on target nuclei noted in column one. Other optical potential parameters, given in Eq. (2), are kept fixed with the values $V_0 = -37.0$ MeV, $a_0 = 0.324$ fm and $a_1 = 0.333$ fm. Our calculated reaction cross sections, σ_r(theor) in millibarns, for both π^+ and π^-, are listed in columns 8.

Nucleus	R_0		V_1		W_3		R_1	R_3	a_3	σ_r (theor)	
	π^+	π^-	π^+	π^-	π^+	π^-		$\pi^{\pm}$		π^+	π^-
Carbon-12	4.00	4.03	150.0	140.0	-210.0	-70.0	3.00	1.70	0.370	100.4	227.4
Oxygen-16	4.15	4.18	180.0	142.0	-300.0	-75.0	3.00	1.87	0.370	123.1	360.4
Silicon-28	4.70	4.75	214.0	171.0	-400.0	-83.0	3.25	2.25	0.420	248.4	641.7
Sulfur-32	4.82	4.92	223.0	179.0	-444.0	-88.0	3.25	2.36	0.420	324.6	754.3
Calcium-40	5.20	5.30	250.0	193.0	-543.0	-100.0	3.54	2.54	0.420	345.4	842.6
Iron-56	5.45	5.74	267.0	218.0	-680.0	-107.0	3.85	2.84	0.420	381.4	1003.0
Nickel-58	5.54	5.80	271.0	221.0	-742.0	-118.0	3.92	2.86	0.420	405.1	1004.7
Zirconium-90	6.20	6.25	310.0	256.0	-1100.0	-150.0	4.50	3.30	0.420	494.4	1129.6

TABLE II. The optical potential parameters R_0 (in fm), V_1 (in MeV), W_3(in MeV), R_1(in fm), R_3(in fm) and a_3(in fm) used in Eq. (2) for 30 MeV incident charged pions on target nuclei noted in column one. Other optical potential parameters, given in Eq. (2), are kept fixed with the values $V_0 = -37.0$ MeV, $a_0 = 0.324$ fm and $a_1 = 0.333$ fm. Our calculated reaction cross sections, σ_r(theor) in millibarns, for both π^+ and π^-, are listed in columns 8.

Nucleus	R_0		V_1		W_3		R_1	R_3	a_3	σ_r (theor)	
	π^+	π^-	π^+	π^-	π^+	π^-		$\pi^{\pm}$		π^+	π^-
Carbon-12	3.85	3.95	129.0	110.0	-120.0	-72.0	3.00	1.70	0.370	107.1	169.5
Oxygen-16	4.00	4.10	155.0	122.0	-175.0	-84.0	3.00	1.87	0.370	137.1	256.3
Silicon-28	4.55	4.69	185.0	147.0	-245.0	-111.0	3.25	2.25	0.420	278.6	473.4
Sulfur-32	4.64	4.82	194.0	154.0	-276.0	-122.0	3.25	2.36	0.420	347.0	563.9
Calcium-40	5.11	5.20	210.0	166.0	-340.0	-140.0	3.54	2.54	0.420	393.0	634.2
Iron-56	5.14	5.48	236.0	186.0	-458.0	-180.0	3.85	2.84	0.420	426.0	769.3
Nickel-58	5.20	5.56	239.0	188.0	-479.0	-193.0	3.92	2.86	0.420	435.9	774.1
Zirconium-90	5.70	6.25	277.0	217.0	-720.0	-280.0	4.50	3.30	0.420	503.3	961.0

TABLE III. The optical potential parameters R_0 (in fm), V_1 (in MeV), W_3(in MeV), R_1(in fm), R_3(in fm) and a_3(in fm) used in Eq. (2) for 40 MeV incident charged pions on target nuclei noted in column one. Other optical potential parameters, given in Eq. (2), are kept fixed with the values $V_0 = -37.0$ MeV, $a_0 = 0.324$ fm and $a_1 = 0.333$ fm. Our calculated reaction cross sections, σ_r(theor) in millibarns, for both π^+ and π^-, are listed in columns 8.

Nucleus	R_0		V_1		W_3		R_1	R_3	a_3	σ_r (theor)	
	π^+	π^-	π^+	π^-	π^+	π^-		$\pi^{\pm}$		π^+	π^-
Carbon-12	3.75	3.95	103.0	90.0	-77.0	-74.0	3.00	1.70	0.370	127.3	141.4
Oxygen-16	3.89	4.05	125.0	100.0	-110.0	-96.0	3.00	1.87	0.370	170.7	201.6
Silicon-28	4.33	4.59	154.0	123.0	-178.0	-134.0	3.25	2.25	0.420	313.7	393.9
Sulfur-32	4.43	4.73	162.0	128.0	-203.0	-151.0	3.25	2.36	0.420	385.5	471.3
Calcium-40	4.75	4.95	180.0	138.0	-245.0	-170.0	3.54	2.54	0.420	403.3	519.4
Iron-56	4.93	5.43	199.0	156.0	-351.0	-234.0	3.85	2.84	0.420	505.1	678.6
Nickel-58	5.00	5.52	200.0	160.0	-366.0	-250.0	3.92	2.86	0.420	512.6	683.2
Zirconium-90	5.55	6.20	235.0	180.0	-563.0	-395.0	4.50	3.30	0.420	633.8	878.0

rameters embedded in our potential within the framework of full Klein-Gordon equation, are achieved and, as such, support our suggested scaling method as a credible benchmark. The general trends of the potential parameters make it possible to predict the parameters for other systems as $\pi^{\pm}$ - ^{28}Si, ^{32}S, ^{56}Fe at the three energies 20, 30 and 40 MeV, $\pi^{\pm}$ - ^{58}Ni

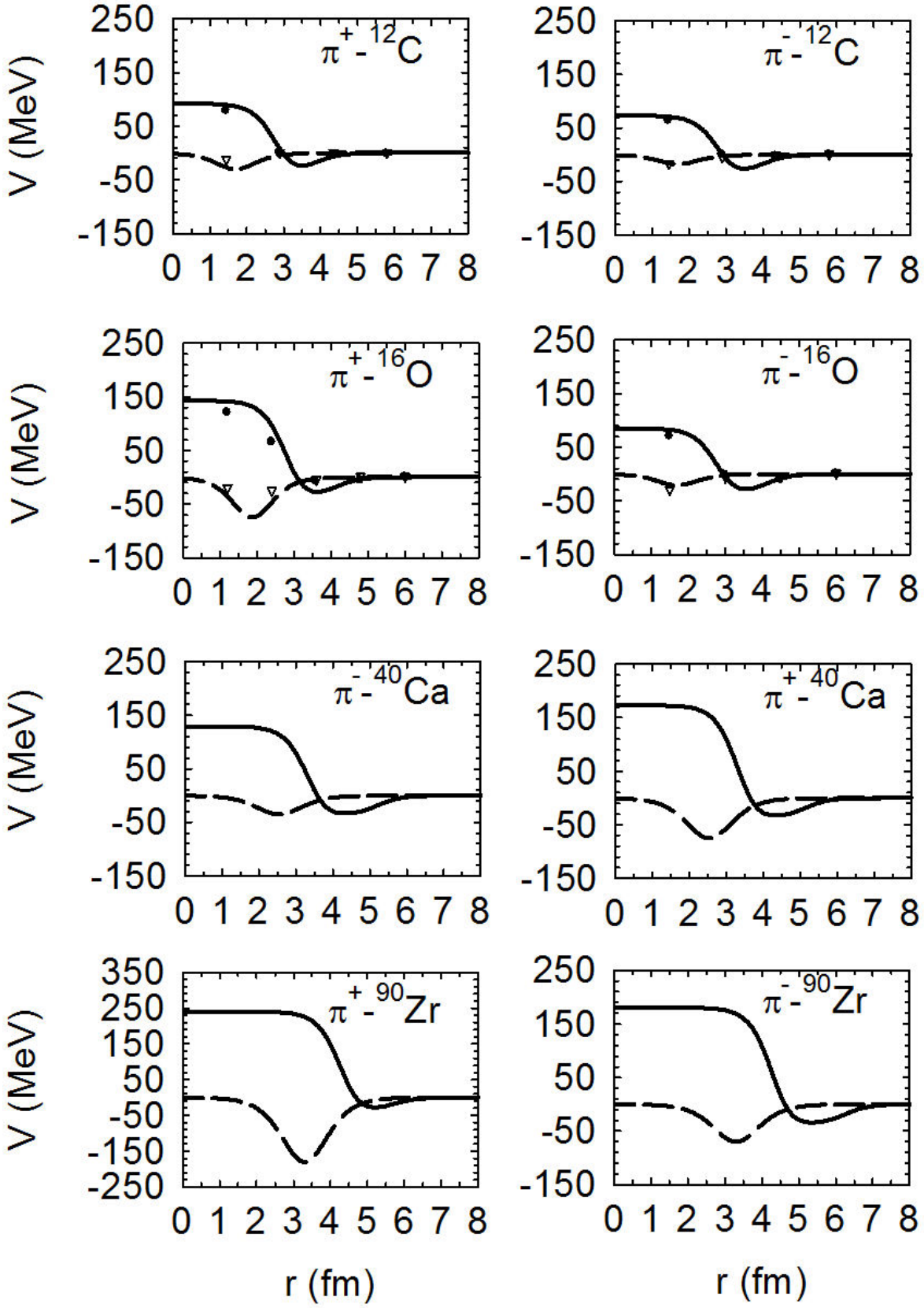

FIGURE 2. Same as Fig. 1 but for 30 MeV. The inverted real and imaginary potential points, obtained from available phase shifts [14,15], are represented by solid circles and empty triangles, respectively.

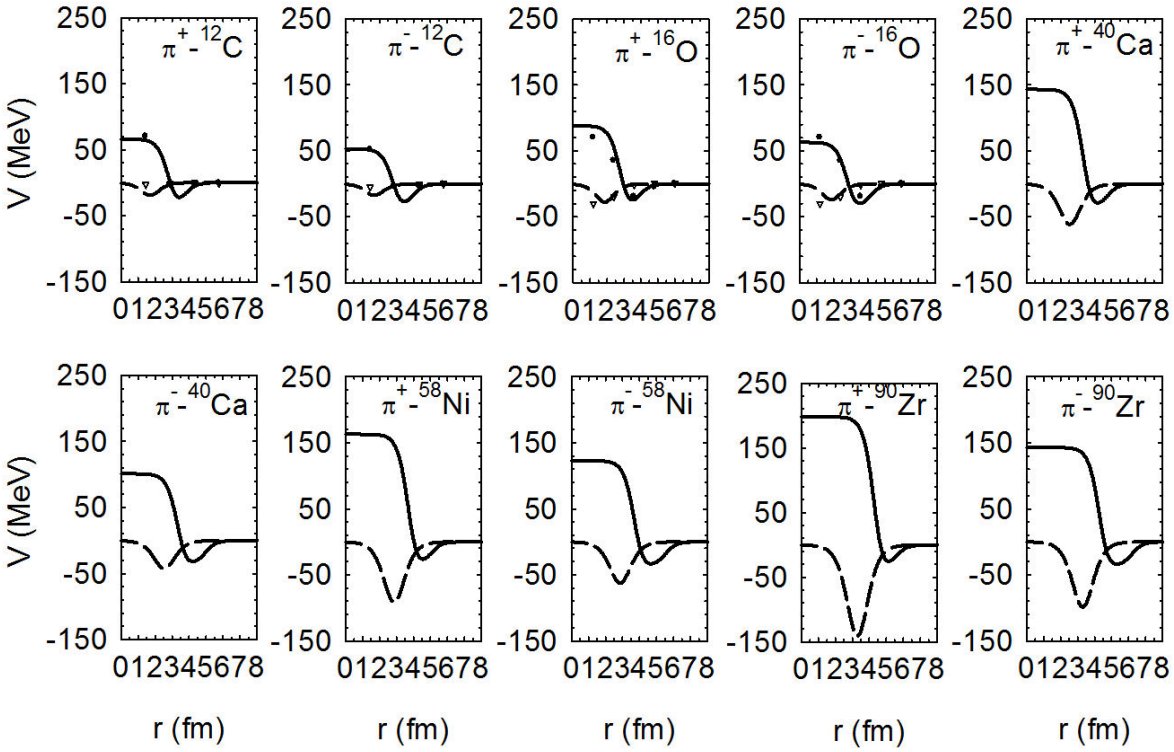

FIGURE 3. Same as Fig. 2 but for 40 MeV. Available phase shifts are taken from Refs. 14 and 15.

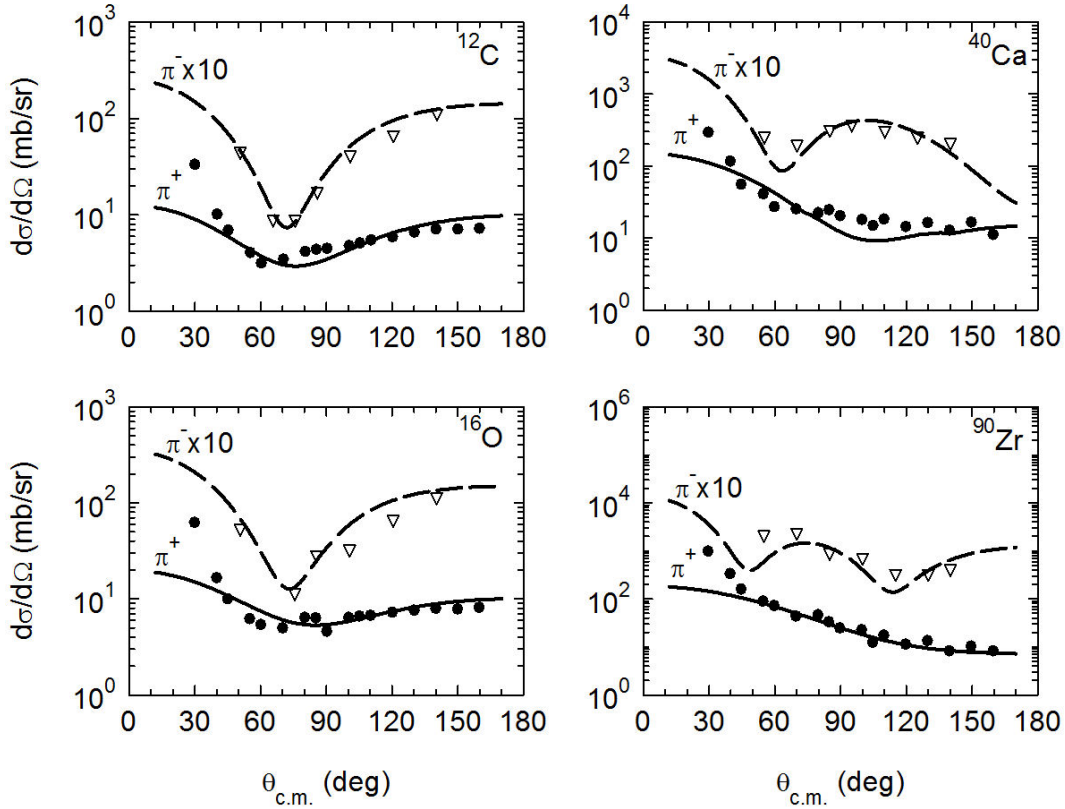

FIGURE 4. The calculated differential cross sections, drawn as solid and dashed lines for positive and negative pions, respectively, compared to the experimental data, represented by solid circles and empty triangles [16,17], as a function of center of mass angle $\theta_{c.m.}$ for 20 MeV incident charged pions scattered off the nuclei ^{12}C, ^{16}O, ^{40}Ca, and ^{90}Zr. The calculations are made by using the scaled potentials, real and imaginary parts, drawn as solid and dashed lines in Fig. 1 for both positive and negative pions, respectively.

at 20 and 30 MeV, π^+ - ^{58}Ni and π^- - ^{90}Zr at 40 MeV. With no doubt, one can use this method in determining potential parameters for other-like nuclear systems as kaon-nucleus systems, which will be thoroughly investigated in the nearest future. To the best of our knowledge, this method is new in pion physics and it deserves special attention and appreciation. The crux of its importance is in explaining low-energy pion-nucleus and, hopefully, kaon-nucleus systems with no available phase shifts.

Based on our previous successful results, and guided by the corresponding obtained scaling relations, we are following the same strategy in determining the potential parameters and in obtaining the associated scaling relations for systems under investigation. The six potential parameters, V_0, a_0, R_1, a_1, R_3 and a_3, are kept as in Ref. 7. The starting values for the other three parameters, R_0, V_1 and W_3, for $\pi^\pm$ - ^{12}C and $\pi^\pm$ - ^{16}O were taken as reported before [5]. For other target nuclei, the values for R_0 and V_1 were first taken following the $(A_2/A_1)^{1/3}$ rule, and W_3 values following the (A_2/A_1) rule. To obtain the best possible agreements between measured and calculated differential cross sections, the values of the three free parameters, R_0, V_1 and W_3, were slightly adjusted. For pion-nucleus scattering cases with available phase shifts, one may notice the good agreements between the scaled potentials, real and imaginary parts, with the inverted potential points obtained by using inverse scattering theory, where available [14,15]. This is illustrated in Figs. 1, 2 and 3 for $T_\pi = 20$, 30, 40 MeV respectively. The potential parameters, phenomenological and scaled, are noted in Tables I, II, and III for $T_\pi = 20$, 30, 40 MeV, respectively. The calculated differential cross sections, using these potentials, are reasonably compared with measured ones [16-21] in Figs. 4, 5, and 6 for $T_\pi = 20$, 30, 40 MeV, respectively. The underestimated measured differential cross sections for $\theta_{c.m} \leq 30^\circ$ may be attributed to Coulomb scattering effects. In general the achieved simultaneous results are good and they make our suggested scaling method very confident. In addition, our calculated reaction cross sections are tabulated for all pion-nucleus systems at all three pion's incident kinetic energies considered herein. The values of these calculated cross sections have a certain trend with both incident pion's kinetic energy, T_π, and the atomic mass of the target nucleus, $A(u)$, in atomic mass units. Unfortunately the available measured values, and the ones calculated by other authors, are uncertain, with no trends, and with a noticeable contradiction [5].

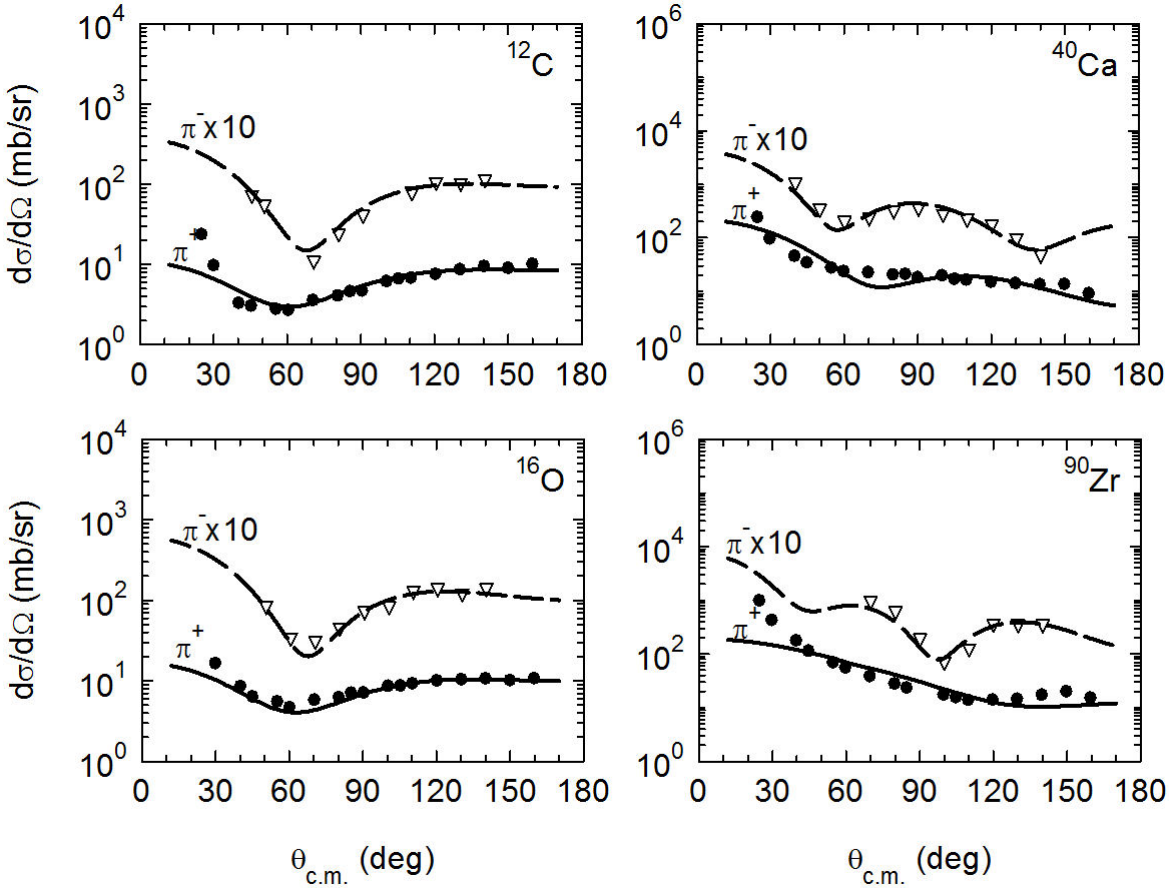

FIGURE 5. The calculated differential cross sections, drawn as solid and dashed lines for positive and negative pions, respectively, compared to the experimental data, represented by solid circles and empty triangles [18,19], as a function of center of mass angle $\theta_{c.m.}$ for 30 MeV incident charged pions scattered off the nuclei ^{12}C, ^{16}O, ^{40}Ca, and ^{90}Zr. The calculations are made by using the scaled potentials, real and imaginary parts, drawn as solid and dashed lines in Fig. 2 for both positive and negative pions, respectively.

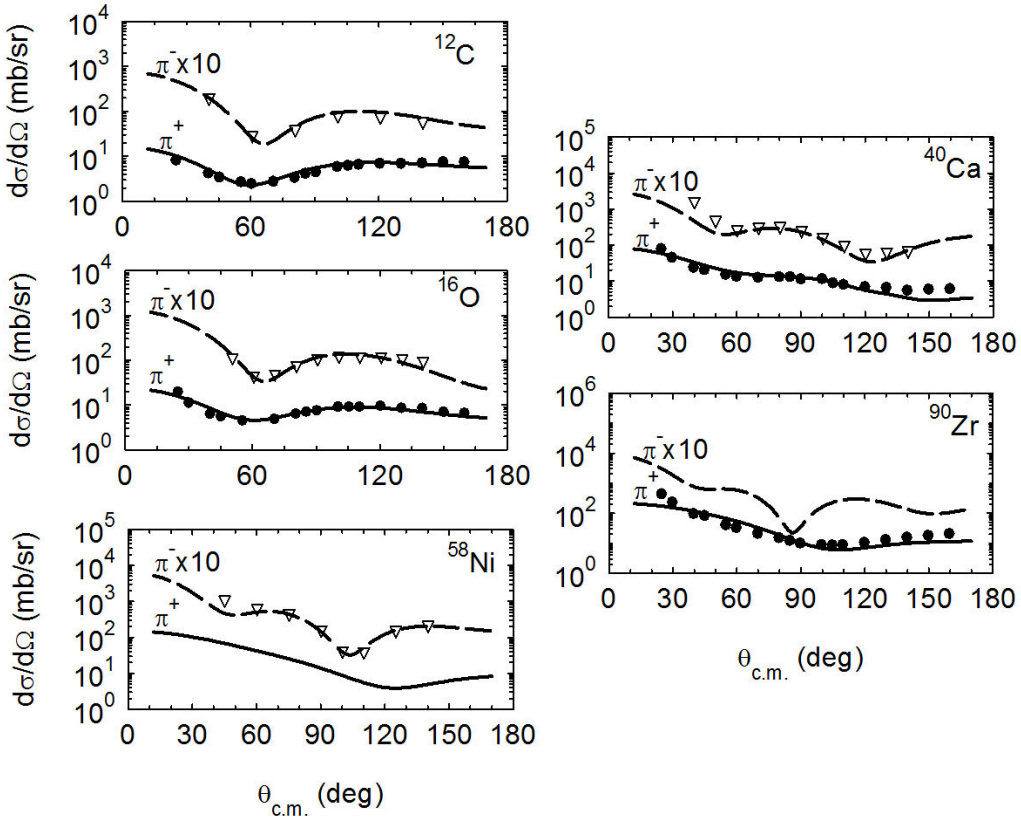

FIGURE 6. The calculated differential cross sections, drawn as solid and dashed lines for positive and negative pions, respectively, compared to the experimental data, represented by solid circles and empty triangles [17, 20, 21], as a function of center of mass angle $\theta_{c.m.}$ for 40 MeV incident charged pions scattered off the nuclei ^{12}C, ^{16}O, ^{40}Ca, ^{58}Ni and ^{90}Zr. The calculations are made by using the scaled potentials, real and imaginary parts, drawn as solid and dashed lines in Fig. 3 for both positive and negative pions, respectively.

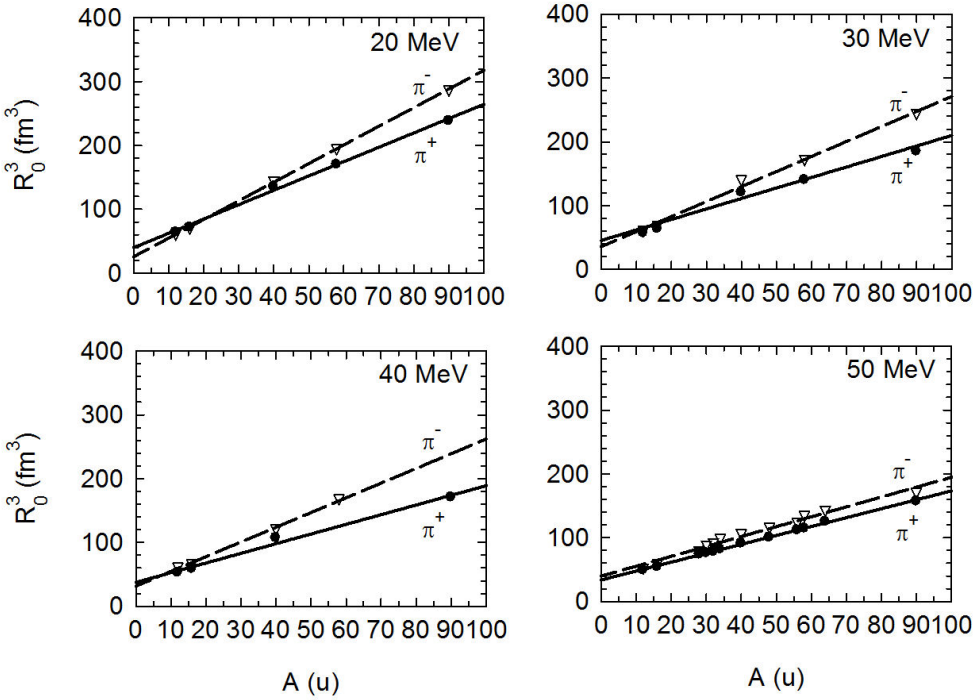

FIGURE 7. The cube of R_0-values versus the atomic mass of the target nucleus in atomic mass units, $A(u)$ for $T_\pi = 20$, 30, 40 MeV and 50 MeV. The R_0-values at 50 MeV are taken from Ref. 7. The solid and dashed lines, for positive and negative pions, respectively, are just to guide the eye.

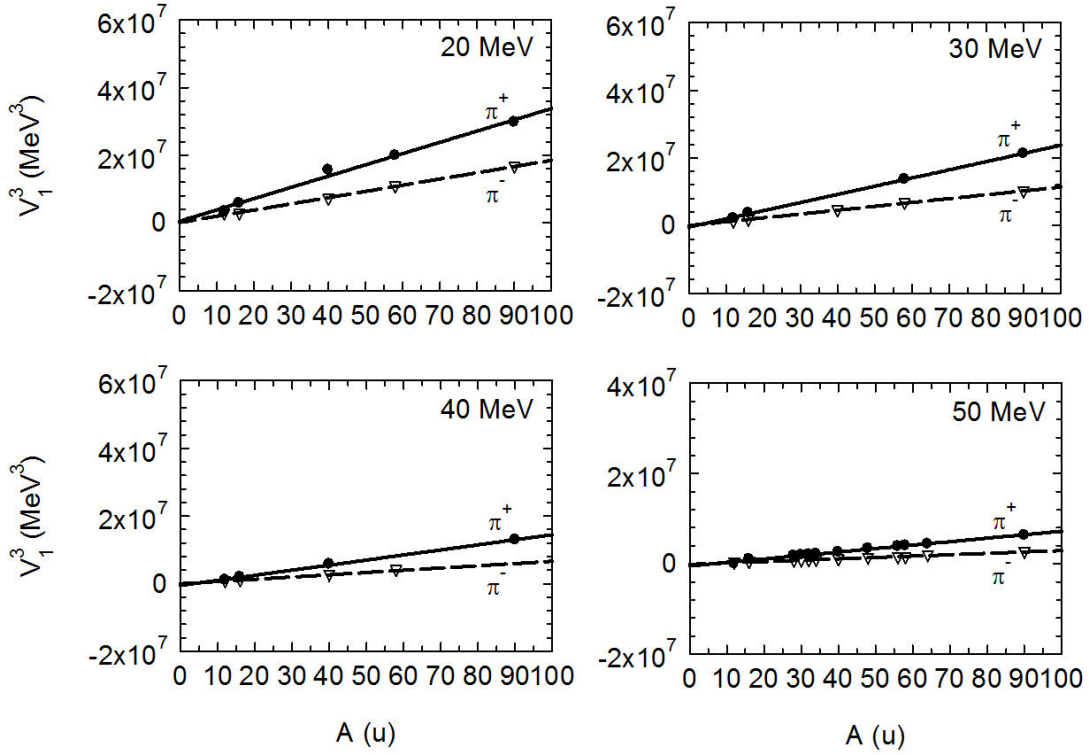

FIGURE 8. The cube of V_1-values versus the atomic mass of the target nucleus in atomic mass units, $A(u)$ for $T_\pi = 20$, 30, 40 and 50 MeV. The V_1-values at 50 MeV are taken from Ref. 7. The solid and dashed lines, for positive and negative pions, respectively, are just to guide the eye.

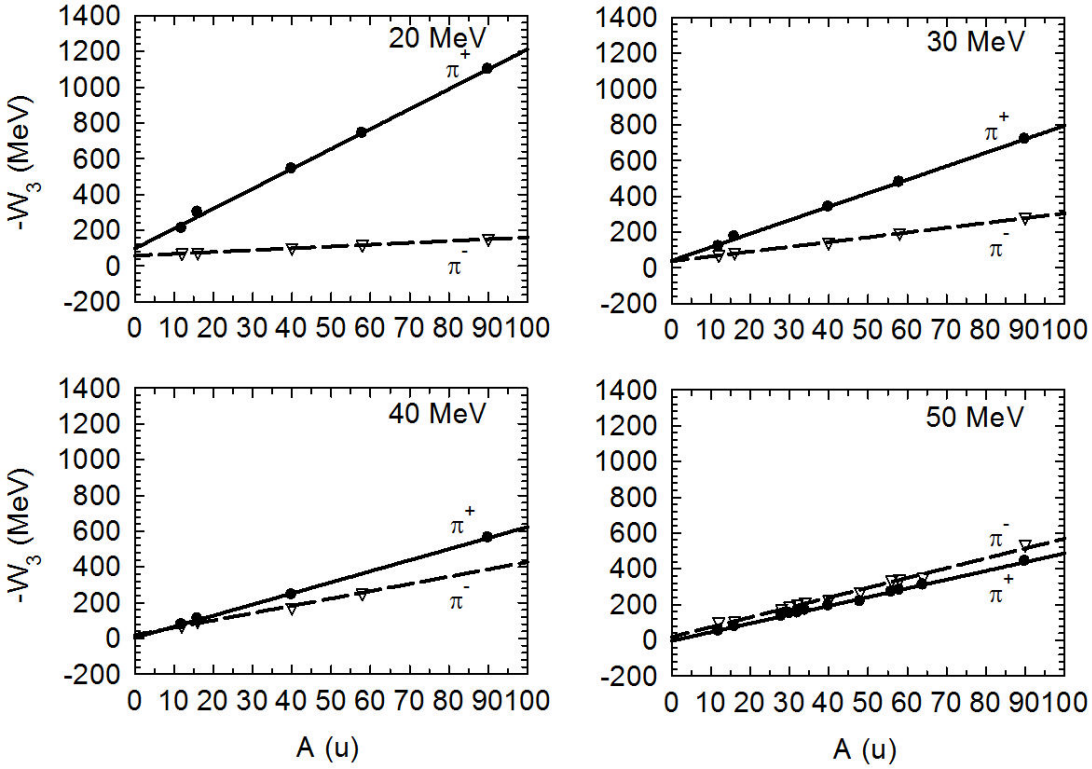

FIGURE 9. The W_3-values versus the atomic mass of the target nucleus in atomic mass units, $A(u)$ for $T_\pi = 20$, 30, 40 and 50 MeV. The W_3-values at 50 MeV are taken from Ref. 7. The solid and dashed lines, for positive and negative pions, respectively, are just to guide the eye.

Our results show clearly that scaled potential parameters depend mainly on the incident pion's kinetic energy, T_π, and the atomic mass of the target nucleus, $A(u)$, in atomic mass units. It is very informative, essential, and of great interest to investigate deeply such a dependence. Figures 7, 8, and 9 show a linear increase of R_0^3, V_1^3, $-W_3$, respectively with $A(u)$ for the three energies considered herein in addition to the values at 50 MeV [7]. This allows to estimate any of these scaled potential parameters for any target nucleus in a low- energy pion-nucleus scattering case. On the contrary, Figs. 10 and 11 show a systematic decrease of R_0 and V_1, respectively, with T_π for π^+ scattered off the four target nuclei ^{12}C, ^{16}O, ^{40}Ca, and ^{90}Zr. Moreover, Fig. 12 shows a curve-like, somewhat quadratic, behavior for $-W_3$ versus T_π. In all these figures, the values at 50 MeV are taken from our recent previous study [7]. Moreover the nine W_3-values, at T_π = 65, 70, 80 MeV for the three target nuclei ^{40}Ca, ^{58}Ni and ^{90}Zr, were extrapolated from those for ^{12}C and ^{16}O [5] as W_3 is connected to A_2/A_1. Although our manuscript is concerned with the three low energies, $T_\pi = 20$, 30, 40 MeV, it is worthy to point out that the inclusion of the values at 50 MeV and the nine W_3-values serves for integrity, completeness, compatibility and comparison reasons. Overall, our results show a good qualitative agreement with our previous ones [5,7].

For positive pions with T_π = 20, 30, 40, 50 MeV, the obtained scaling relations for the three potential parameters with the atomic mass number are, respectively:

$$R_0^3 = 2.25A + 39.9 \ \ (\text{fm}^3),$$
$$V_1^3 = 3.33 \times 10^5 A + 5.34 \times 10^5 \ \ (\text{MeV})^3,$$
$$W_3 = -11.1A - 98.00 \ \ (\text{MeV}) \qquad (14a)$$

$$R_0^3 = 1.64A + 45.5 \ \ (\text{fm}^3),$$
$$V_1^3 = 2.42 \times 10^5 A - 4.41 \times 10^5 \ \ (\text{MeV})^3,$$
$$W_3 = -7.55A - 40.70 \ \ (\text{MeV}) \qquad (14b)$$

$$R_0^3 = 1.52A + 37.5 \ \ (\text{fm}^3),$$
$$V_1^3 = 1.50 \times 10^5 A - 5.08 \times 10^5 \ \ (\text{MeV})^3,$$
$$W_3 = -6.19A - 4.740 \ \ (\text{MeV}) \qquad (14c)$$

$$R_0^3 = 1.40A + 33.8 \ \ (\text{fm}^3),$$
$$V_1^3 = 0.767 \times 10^5 A - 4.52 \times 10^5 \ \ (\text{MeV})^3,$$
$$W_3 = -4.89A - 2.630 \ \ (\text{MeV}) \qquad (14d)$$

and for negative pions with T_π = 20, 30, 40, 50 MeV the obtained scaling relations for the three potential parameters with the atomic mass number are, respectively:

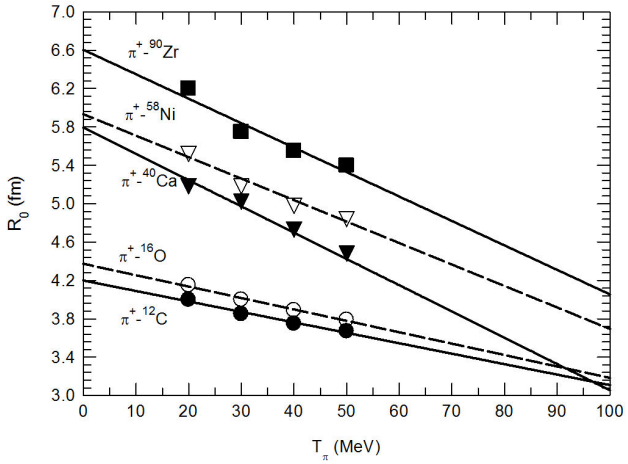

FIGURE 10. The R_0-values versus the incident pion's kinetic energy, T_π(MeV) for five different target nuclei. The R_0-values at 50 MeV are taken from Ref. 7. The solid and dashed lines are just to guide the eye.

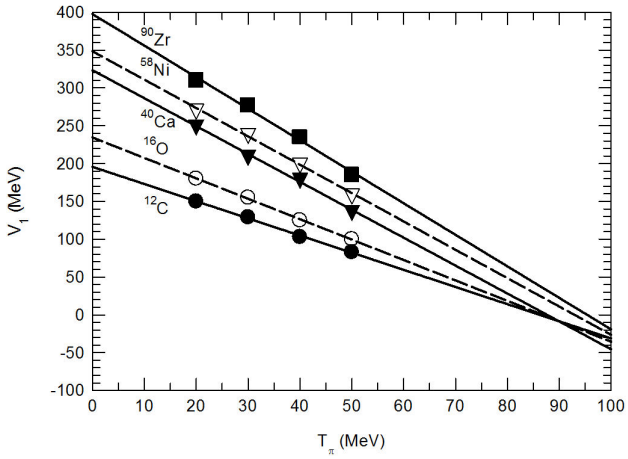

FIGURE 11. The V_1-values versus the incident pion's kinetic energy, T_π(MeV) for positive pions scattered off five different target nuclei. The V_1-values at 50 MeV are taken from ref. [7]. The solid and dashed lines are just to guide the eye.

$$R_0^3 = 2.92A + 25.6 \ \ (\text{fm}^3),$$
$$V_1^3 = 1.84 \times 10^5 A + 1.46 \times 10^5 \ \ (\text{MeV})^3,$$
$$W_3 = -1.02A - 58.50 \ \ (\text{MeV}) \qquad (15a)$$

$$R_0^3 = 2.35A + 35.8 \ \ (\text{fm}^3),$$
$$V_1^3 = 1.14 \times 10^5 A - 0.06536 \times 10^5 \ \ (\text{MeV})^3,$$
$$W_3 = -2.67A - 38.00 \ \ (\text{MeV}) \qquad (15b)$$

$$R_0^3 = 2.30A + 371.6 \ \ (\text{fm}^3),$$
$$V_1^3 = 0.664 \times 10^5 A - 0.197 \times 10^5 \ \ (\text{MeV})^3,$$
$$W_3 = -4.08A - 20.10 \ \ (\text{MeV}) \qquad (15c)$$

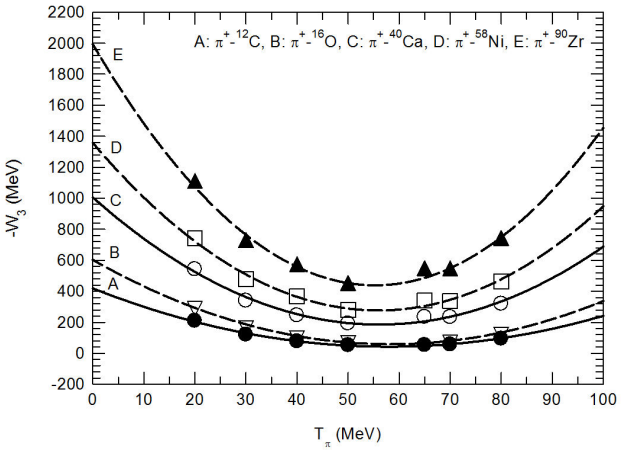

FIGURE 12. The W_3-values versus the incident pion's kinetic energy, T_π(MeV) for five different target nuclei. The W_3-values at 50 MeV are taken from Ref. 7 and the W_3-values at energies greater than 50 MeV are extrapolated.. The solid and dashed lines are just to guide the eye.

$$R_0^3 = 1.55A + 3939 \ \ (\text{fm}^3),$$
$$V_1^3 = 0.306 \times 10^5 A - 1.30 \times 10^5 \ \ (\text{MeV})^3,$$
$$W_3 = -5.49A - 19.80 \ \ (\text{MeV}) \qquad (15d)$$

For positive pions, the obtained scaling relations for the three potential parameters with the pion's incident kinetic energy, for the five target nuclei under consideration, are, respectively :

$$^{12}\text{C} : R_0 = -0.0109T_\pi + 4.20 \ \ (\text{fm}),$$
$$V_1 = -2.27T_\pi + 196 \ \ (\text{MeV}),$$
$$-W_3 = 0.112T_\pi^2 - 13.0T_\pi + 419 \ \ (\text{MeV}) \qquad (16a)$$

$$^{16}\text{O} : R_0 = -0.0119T_\pi + 4.37 \ \ (\text{fm}),$$
$$V_1 = -2.70T_\pi + 235 \ \ (\text{MeV}),$$
$$-W_3 = 0.160T_\pi^2 - 18.7T_\pi + 603 \ \ (\text{MeV}) \qquad (16b)$$

$$^{40}\text{Ca} : R_0 = -0.0274T_\pi + 5.79 \ \ (\text{fm}),$$
$$V_1 = -3.69T_\pi + 323 \ \ (\text{MeV}),$$
$$-W_3 = 0.261T_\pi^2 - 29.2T_\pi + 1005 \ \ (\text{MeV}) \qquad (16c)$$

$$^{58}\text{Ni} : R_0 = -0.0224T_\pi + 5.93 \ \ (\text{fm}),$$
$$V_1 = -3.75T_\pi + 349 \ \ (\text{MeV}),$$
$$-W_3 = 0.345T_\pi^2 - 38.6T_\pi + 1357 \ \ (\text{MeV}) \qquad (16d)$$

$$^{90}\text{Zr} : R_0 = -0.0255T_\pi + 6.60 \ \ (\text{fm}),$$
$$V_1 = -4.17T_\pi + 398 \ \ (\text{MeV}),$$
$$-W_3 = 0.508T_\pi^2 - 56.2T_\pi + 1993 \ \ (\text{MeV}) \qquad (16e)$$

4. Conclusions

This study confirms the suitability of the scaling method in obtaining potential parameters for a certain pion-nucleus system from a nearby one. This method is unique for low-energy pion-nucleus systems with no available shifts. The good agreements between calculated and measured differential cross sections, for different pion-nucleus systems at three low energies, represent a strong indication on the success of the method. Nevertheless, the analytical forms of our potentials agree with the inverted potential points where available. On the otherhand, and even with no available experimental reaction cross sections for most of the cases under consideration, or uncertain values for few of them, our calculated values are included, pending for future measured precise values. We believe that the results of this study, accompanied with the results of our two recent related studies, based on the scaling method are suitable to be submitted for a patent. In view of this, our scaling method will be used in analyzing low-energy kaon-nucleus elastic-scattering data. It is also tempted that this study, especially at 20 MeV, will positively contribute in accounting for pionic atom data and, then, in investigating pionic atom physics.

Acknowledgments

The authors are very pleased to acknowledge the encouragement and financial support of the Deanship of Scientific Research at Taif University for carrying out this investigation. Our thanks are extended to Professors A. K. Basak and M. S. Abu-Jafar for illuminating discussions, and for sharing their computer expertise.

1. Z. F. Shehadeh, *J. Assoc. Arab Univ. Basic Appl. Sci.* **14** (2013) 32-37.
2. R. M. Al-Shawaf and Z. F. Shehadeh, *Int. J. Phys. Sci*. **11** (2016) 85-95.
3. C. M. Chen, D. J. Ernst and M. B. Johnson, *Phys. Rev. C* **48** (1993) 84-849.
4. E. Friedman, *Acta Physica Polonica B* **24** (1993) 1673-1684.
5. Z. F. Shehadeh and R. M. El-Shawaf, *Rev. Mex. Fis.* **62** (2016) 475-483.
6. Z. F. Shehadeh, *Int. J. Mod. Phys. E* **18** (2009) 1615-1627.
7. Z. F. Shehadeh and R. M. El-Shawaf, *Rev. Mex. Fis.* **63** (2017) 230-237.
8. H. M. Pilkuhn, *Relativistic Particle Physics*, (Springer-Verlag, New York, 1979).
9. W. R. Gibbs, *Computations in Modern Physics*, (World Scientific, New York, 2006).
10. R. A. Eisenstein and G. A. Miller, *Comp. Phys. Commun*. **8** (1974) 130-140.
11. P. Manngard, M. Brenner, M. M. Alam, I. Reichstein and F. B. Malik, *Nucl. Phys. A* **504** (1989) 130-142.
12. Q. Haider and F. B. Malik, *J. Phys. G: Nucl. Phys.* **7** (1981) 1661-1669.
13. Z. F. Shehadeh, *Non-relativistic nucleus-nucleus and relativistic pion-nucleus interactions*, Ph. D. Thesis Southern Illinois University at Carbondale, (1995).
14. J. Fröhlich, H. G. Schlaile, L. Streit and H. Zingl, *Z. Phys. A-Atoms and Nuclei* **302** (1981) 89-94.
15. O. Dumbrajs, J. Fröhlich, U. Klein and H. G. Schlaile, *Phys. Rev. C* **29** (1984) 581-591.
16. F. E. Obenshain *et al*., *Phys. Rev. C* **27** (1983) 2753-2758.
17. G. Burleson *et al*., *Phys. Rev. C* **49** (1994) 2226-2229.
18. K. K. Seth *et al*., *Phys. Rev. C* **41** (1990) 2800-2808.
19. B. M. Preedom *et al*., *Phys. Rev. C* **23** (1981) 1134-1140.
20. M. Blecher *et al*., *Phys. Rev. C* **20** (1979) 1884-1890.
21. D. J. Malbrough *et al.*, *Phys .Rev. C* **17** (1978) 1395-1401.